Supplemental Document

optica

High-power few-cycle Cr:ZnSe mid-infrared source for attosecond soft x-ray physics: supplement

VYACHESLAV E. LESHCHENKO,[1,*] BRADFORD K. TALBERT,[1] YU HANG LAI,[1] SHA LI,[1] YAGUO TANG,[1] STEPHEN J. HAGEMAN,[1] GREG SMITH,[1] PIERRE AGOSTINI,[1] LOUIS F. DIMAURO,[1] AND COSMIN I. BLAGA[1,2]

[1]*Department of Physics, The Ohio State University, Columbus, Ohio 43210, USA*
[2]*Department of Physics, Kansas State University, Manhattan, Kansas 66506, USA*
[*]*Corresponding author: leshchenko.1@osu.edu*

This supplement published with The Optical Society on 10 August 2020 by The Authors under the terms of the Creative Commons Attribution 4.0 License in the format provided by the authors and unedited. Further distribution of this work must maintain attribution to the author(s) and the published article's title, journal citation, and DOI.

Supplement DOI: https://doi.org/10.6084/m9.figshare.12459062

Parent Article DOI: https://doi.org/10.1364/OPTICA.393377

High-power few-cycle Cr:ZnSe mid-infrared source for attosecond soft x-ray physics: supplementary material

VYACHESLAV E. LESHCHENKO[1,*], BRADFORD K. TALBERT[1], YU HANG LAI[1], SHA LI[1], YAGUO TANG[1], STEPHEN J. HAGEMAN[1], GREG SMITH[1], PIERRE AGOSTINI[1], LOUIS F. DIMAURO[1], AND COSMIN I. BLAGA[1,2]

[1]*Department of Physics, The Ohio State University, Columbus, Ohio 43210, USA*
[2]*Department of Physics, Kansas State University, Manhattan, Kansas 66506, USA*
[*]*Corresponding author: leshchenko.1@osu.edu*

Compiled June 7, 2020

This document provides supplementary information to "High-power few-cycle Cr:ZnSe mid-infrared source for attosecond soft x-ray physics." In this supplement, we present technical details on the performed simulations and additional experimental results supporting the paper.

1. AMPLIFIER

A. Estimation of the nonlinear phase in the amplifier

ZnSe has a relatively high nonlinear refractive index of about 10^{-14} cm^2/W at 2400 nm [1, 2], which is almost two orders of magnitude higher compared to sapphire for example. Therefore, a careful amplifier design requires an estimation of potentially detrimental nonlinear effects, which can be reduced by choosing an appropriate pulse stretching factor. The standard parameter, which is used to evaluate the influence of nonlinear effects, is the B-integral (total accumulated on-axis nonlinear phase shift), which is determined by the equation

$$B = k \int_0^L n_2 I(z) dz \tag{S1}$$

where k is the wavenumber, n_2 is the nonlinear refractive index, I is the peak intensity, and L is the material length. The condition of $B > 1$ typically determines the threshold for nonlinear effects, hence $B < 1$ should be satisfied in an amplifier.

In the evaluation we assume the stretched pulse duration of 300 ps, which is calculated based on the stretcher geometry (600 lines/mm, 57° angle of incidence, -30 cm effective grating separation) and the seed spectrum. The beam diameter (on the e^{-2} intensity level) is 3.5 mm and the pulse energy is 0.05, 0.5, 3 and 8.2 mJ in the seed and after the first, second and third passes respectively. To simplify the estimation, the mean value between the input and the output energies is used on each pass which should result is a slight overestimation since most of the energy is accumulated at the end of the crystal. The estimated B-integral is 0.7, which is low enough to prevent nonlinear distortions of amplified pulses

B. Stability of the nonimaging amplifier setup (beam size dependence on the thermal lens)

In the implemented (and presented in the paper) nonimaging amplifier geometry, if the thermal lens in the gain element is too strong, the beam can be demagnified to a size resulting in damaging of optics. Therefore, we have performed an estimation of safe limits for the thermal lens in the gain element (though there is no problems with the beam quality and optics damaging in the amplifier presented in the paper).

The telescope in the seed beam before the amplifier was adjusted for the beam to have a waist on the entrance of the crystal. The beam waist diameter after the first pass is determined by the pump beam size of 3.5 mm as written in the main text. Therefore, the simulations are starting from a Gaussian beam with diameter (on e^{-2} intensity level) of 3.5 mm and an infinite radius of phase curvature. The propagation is modeled using the "ABCD law" and the "complex beam parameter" formalism [3]. The gain element is modeled as a thick lens with the thickness of 48 mm and with the radius of curvature of both sides of

$$R = 2(n-1)F \tag{S2}$$

with the refractive index (n) of 2.44, which corresponds to the ZnSe refractive index at 2400 nm. F is the nominal focal length used in the following. The ABCD matrix for a thick lens of

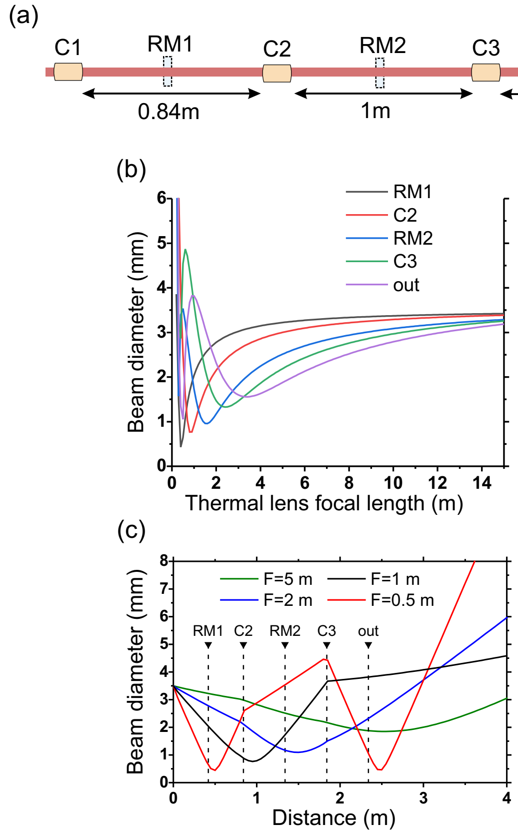

Fig. S1. Simulated beam diameter on the amplifier optics for different focal length of the thermal lens. **a**. Scheme of the simulated optical setup. C stands for the crystal (C1, C2, C3: first, second and third pass respectively), RM for roof mirrors, and 'out' for the output coupler. Note that physically there is only one crystal as shown in the experimental scheme in the paper (Fig. 1), and the beam is directed back to the same crystal with a pair of flat mirrors labeled as RM (roof mirror); each roof mirror is positioned half way between the passes. Each crystal is modeled as a thick lens (see text for details); between the crystal passes the beam is traced using a free-space propagation matrix. **b**. Beam sizes on optical elements (see labels in (a)) for different focal lengths of the thermal lens in the gain element. **c**. Beam size at different positions in the amplifier for a set of focal lengths of the gain element. Note that for any focal length of $\geqslant$ 1 m the fluence on all optical elements is below the damage threshold.

thickness d is

$$M = \begin{bmatrix} 1 & 0 \\ -\frac{n-1}{R} & n \end{bmatrix} \begin{bmatrix} 1 & d \\ 0 & 1 \end{bmatrix} \begin{bmatrix} 1 & 0 \\ -\frac{n-1}{nR} & \frac{1}{n} \end{bmatrix} \qquad \text{(S3)}$$

The complete set of simulated optical elements is shown in Fig. S1(a). The simulation results (Fig. S1(b-c)) indicate that the beam never "collapses" (focuses to a very small diameter) for any focal length of the thermal lens of larger than 1 m, when the fluence on all elements is above the damage threshold (which is at least 1 J/cm^2 for the Cr:ZnSe crystal and >2 J/cm^2 for mirrors). For example, on the output mirror, where the energy is the highest, the minimum beam size (for f=3.35 m) is 1.54 mm, which corresponds to the peak fluence of 0.88 J/cm^2 at the highest obtained power of 8.2 W (peak fluence is the fluence at the center

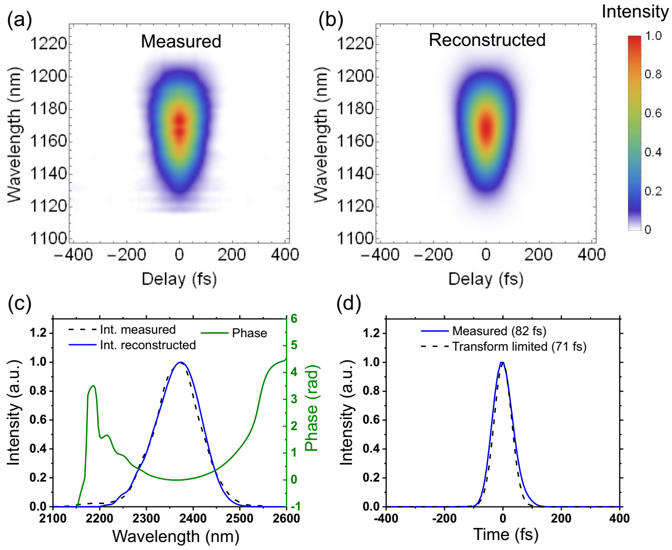

Fig. S2. Seed compression results. **a**. Measured FROG trace. **b**. Reconstructed FROG trace. The reconstruction error is 0.002. **c**. Measured and reconstructed spectra and spectral phase. “Int.” in the legend stand for intensity. **d**. Temporal intensity profile of the pulse.

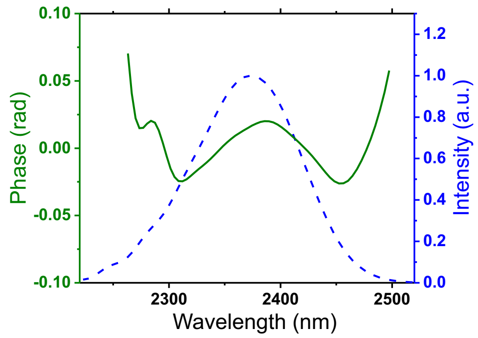

Fig. S3. Residual seed phase (green) after subtracting second and third order dispersion. Seed spectrum is shown in blue dashed line for reference.

of the beam), which is adequately below the damage threshold. As the beam size in the experimentally realized setup was above 2 mm, we conclude that the thermal lens in the amplifier crystal was larger than ∼5 m. At lower pump power and larger focal length of the corresponding thermal lens, the operation of the amplifier is completely robust, since the beam sizes on the optics in the amplifier are converging to the input beam size of 3.5 mm, as clearly seen in Fig. S1(b). It is the consequence of the fact that the Rayleigh length of the seed pulse of 4 m is larger than the entire path in the amplifier. Presented analysis supports the statement in the main text that the amplifier is absolutely stable and safe to operate at any available pump power.

C. Temporal characterization of seed pulses before the stretcher

In order to exclude the influence of the seed spectral phase inherited from the OPA setup on the compression of amplified pulses, the pulses before the stretcher were characterized using the SHG-FROG diagnostics. The measured FROG trace of seed pulses and the reconstruction results are presented in Fig. S2.

The seed pulse is slightly chirped from 71 fs (transform limit) to 82 fs, but the spectral phase is mostly defined by the second order dispersion (which is also clear from the FROG trace that has no sign of any significant high order dispersion). Since the second and third order chirp in the entire stretcher-amplifier-compressor setup can be eliminated by optimizing the angle of incidence and gratings separation in the compressor, the contribution of the seed phase to the residual phase of the amplified pulses (Fig. 3(c) in the main text) can be calculated by subtracting the second and third order components from the measured seed spectral phase (Fig. S2(c)). To do so, the detected phase was interpolated with a third order polynomial within the spectral interval where the normalized intensity is higher than e^{-2}. The result after subtracting the polynomial fit from the measured spectral phase is shown in Fig. S3. The amplitude of phase deviations is about 0.05 rad which is 20 times smaller than in the measured spectral phase of the amplified pulses (where it is about 1 rad). Thus, the contribution of the seed phase to the uncompensated phase of the amplified pulses is negligible.

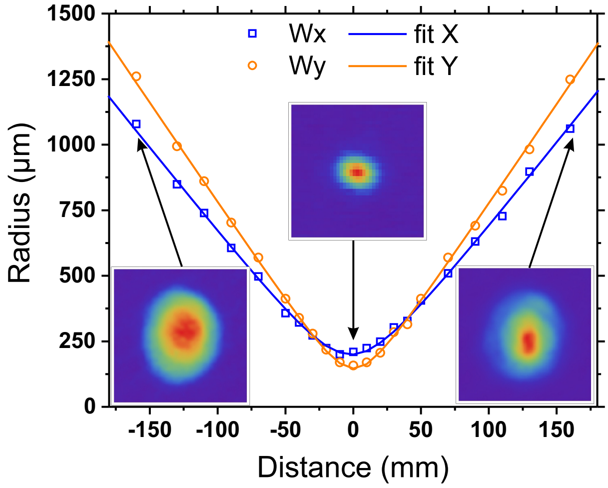

Fig. S4. Beam profile after the nonlinear compression (see the experimental setup in Fig. 5(a) in the main text) and M^2 measurement results with $M_x^2 = 1.7$ and $M_y^2 = 1.46$.

2. NONLINEAR COMPRESSION

A. Details on the simulation of the nonlinear compression

The simulation result presented in Fig. 5(d) (black curve) in the main text was obtained with a one-dimensional (1D)+time split-step method, which follows an approach similar to [4]. In the simulation, the beam propagates through a sequence of the materials in accordance with the experimental scheme shown in Fig. 5(a) in the main text, including an additional 2 m of air propagation to the FROG setup. All lenses were simulated as CaF_2 substrates with 3 mm thickness, which corresponds (with minor variations) to the central thickness of all the installed lenses. The temporal and spectral characteristics of the input pulse were taken from the reconstruction results of the measured FROG trace (Fig. 3 in the main text). The fluence on each optical element was estimated by measuring the corresponding beam profiles. Because of the small thickness of the substrates and the long Rayleigh-length of the beam, the fixed fluence was assumed on each step; for the same reason effects like walk-off, diffraction and self-focusing can be neglected, and 1D simulation should give a meaningful result. Since air has much lower nonlinearity compared to CaF_2 substrates and the beam size was large in air propagation parts, air nonlinearity was neglected. However, air dispersion and absorption were taken into account. The obtained simulation result is shown in Fig. 5(d) (black curve) and demonstrates a reasonably good agreement with experimental data.

In addition, a better optimization of the pulse compression before the nonlinear post-compression stage should result in shortening of the output pulse to about 20 fs in the same experimental setup, according to performed simulations with a flat spectral phase of the input pulse. 20 fs pulse duration at 2.4 µm wavelength corresponds to 2.5 optical cycles, which should enable phase dependent strong field studies and generation of isolated attosecond pulses. The optimization of the compression of the CPA system output can be achieved by implementing, for example, chirped mirrors compensating the dispersion of the gain medium which is the main limiting factor in the present setup.

B. Nonlinear compression limit

In the scheme shown in the paper (Fig. 5(a)) the compression is mostly limited by two parameters: uncompensated spectral phase of the input pulse (as already discussed in the previous section) and the damage threshold of the lenses (Thorlabs lenses were used: E-coated CaF_2 plano-concave and D-coated CaF_2 plano-convex). The damage threshold limits the maximum intensity and correspondingly maximum B-integral per lens, since the thickness of the used Thorlabs lenses is also fixed at about 3 mm. As written in the previous section, better compensation of the spectral phase of the amplified pulses will potentially enable the reduction of the duration of the nonlinear compressed pulses to about 20 fs. In addition, an extra compression stage (a pair of defocussing and focusing lenses) can be introduced to further compress pulses to about 12–15 fs. In this case, the main limiting factor will be temporal pulse front distortions in the focusing lenses [5]. Note that only focusing lenses introduce an appreciable amount of distortion due to the significantly larger beam sizes on them. In particular, the L2 lens (as labeled in Fig.5(a) in the main text) introduces the pulse front curvature corresponding to the delay of 4 fs [5] between the center of the beam and the e^{-2} radius of 4 mm; for L4 this distortion is 8 fs (beam radius is 8.5 mm). Therefore, extra compression stages (pairs of defocussing and focusing lenses) will not improve compression significantly, though they can be advantages for further improvement of spatial homogeneity.

Further significant improvements in pulse shortening are possible by replacing focusing lenses with focusing mirrors. It should enable compression down to ultimately single cycle pulse duration, but a detailed discussion of this scheme is outside of the scope of this paper.

C. Beam quality after nonlinear post-compression

Fig. S4 demonstrates the beam quality (M^2) measurement on the output of the nonlinear post-compression setup presented in the main text. The quality of the post-compressed beam slightly degrades compared to the input beam, namely M^2 increases from about 1.2 to about 1.5. For most of the potential applications, the corresponding slight increase of the focal beam size can be easily compensated by implementing a tighter focusing geometry. The slightly stronger degradation of the beam quality in x-direction is caused mostly by the first YAG plate at the Brewster angle (see experimental setup in Fig. 5(a) of the main text). However,

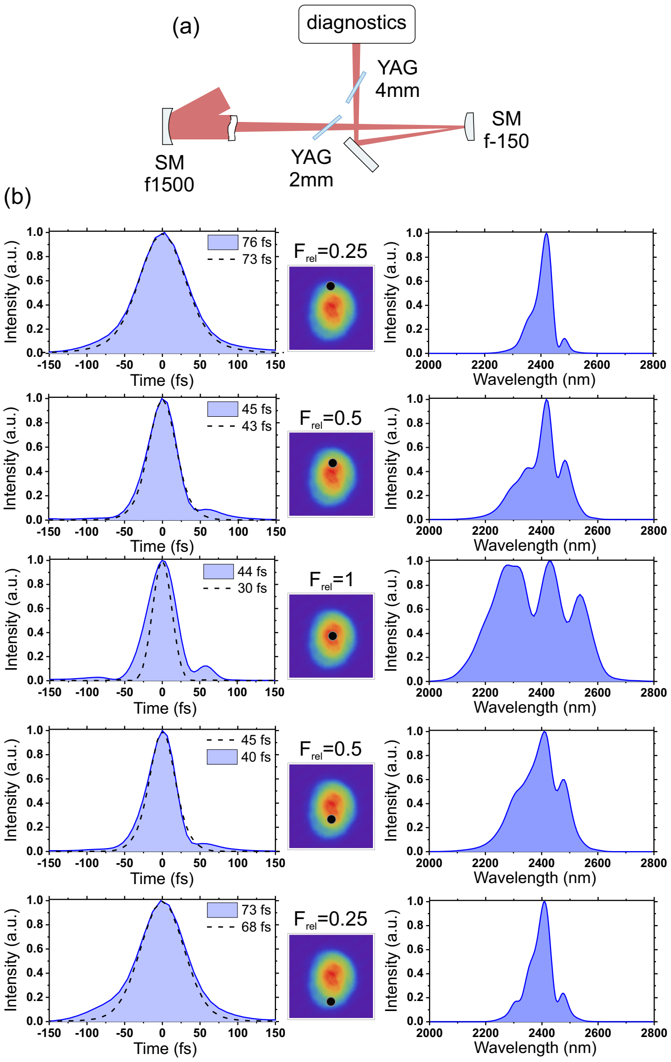

Fig. S5. **a**. Nonlinear compression setup. SM: spherical mirror. **b**. Homogeneity of the nonlinear compression. The measured dependence of the spectrum and pulse duration across the beam profile by selecting a small part of the beam with an aperture indicated as a black circle in the **middle row**. F_{rel} is the fluence in the aperture relative to the peak fluence. **Left row**: temporal pulse profile retrieved from the measured SHG-FROG; blue: measured pulse, black dashed line: transform limited pulse. **Right row**: measured spectrum.

replacing it with an anti-reflection coated substrate near normal incidence will solve the problem.

D. Nonlinear compression in substrates

As mentioned in the main text of the paper, compared to a single-substrate nonlinear compression demonstrated in the mid-IR spectral range at a multi-mJ energy level [6], our approach offers much better spatial homogeneity and beam quality while preserving simplicity and compactness. Here we present an experimental proof of the superiority of the approach presented in the paper. Fig. S5 demonstrates results of the nonlinear compression in a couple of plane-parallel YAG substrates (same material and similar thickness as in [6]) under otherwise similar to the main paper conditions, which enables direct comparison of the techniques. As expected, Fig. S5 clearly demonstrates more pronounced spatio-spectral/temporal inhomogeneity. In particular, the pulse duration increases from 44 fs to sub-80 fs from the center to the edge of the beam, while in a more advanced scheme presented in the paper the inhomogeneity is twice lower: from 40 fs to 60 fs from the center to the edge of the beam. Thus, the nonlinear compression approach introduced in the paper enables significantly better spatial homogeneity and beam quality of multi-mJ mid-IR pulses compared to the previously published results.

REFERENCES

1. A. Major, J. S. Aitchison, P. W. E. Smith, E. Sorokin, and I. T. Sorokina, "Z-scan characterization of the nonlinear refractive index of single crystal ZnSe in the 1.20-1.95 μm wavelength range," in *Photonic Applications in Nonlinear Optics, Nanophotonics, and Microwave Photonics*, vol. 5971 R. A. Morandotti, H. E. Ruda, and J. Yao, eds., International Society for Optics and Photonics (SPIE, 2005), pp. 101 – 108.
2. M. Durand, A. Houard, K. Lim, A. Durécu, O. Vasseur, and M. Richardson, "Study of filamentation threshold in zinc selenide," Opt. Express **22**, 5852–5858 (2014).
3. H. Kogelnik, "Imaging of optical modes — resonators with internal lenses," Bell Syst. Tech. Journal, The **44**, 455–494 (1965).
4. A. Kessel, S. A. Trushin, N. Karpowicz, C. Skrobol, S. Klingebiel, C. Wandt, and S. Karsch, "Generation of multi-octave spanning high-energy pulses by cascaded nonlinear processes in BBO," Opt. Express **24**, 5628–5637 (2016).
5. Z. Bor, "Distortion of femtosecond laser pulses in lenses," Opt. Lett. **14**, 119–121 (1989).
6. V. Shumakova, P. Malevich, S. Ališauskas, A. Voronin, A. M. Zheltikov, D. Faccio, D. Kartashov, A. Baltuška, and A. Pugžlys, "Multi-millijoule few-cycle mid-infrared pulses through nonlinear self-compression in bulk," Nat. Commun. **7**, 12877 (2016).